CO_2 and CH_4 conversion in “real” gas mixtures in a gliding arc plasmatron : how do N_2 and O_2 affect the performance?

CO_2 and CH_4 conversion in "real" gas mixtures in a gliding arc plasmatron: How do N_2 and O_2 affect the performance?

Joachim Slaets,*[a] Maryam Aghaei,[a] Sara Ceulemans,[a] Senne Van Alphen[a] and Annemie Bogaerts*[a]

In this paper we study dry reforming of methane (DRM) in a gliding arc plasmatron (GAP) in the presence of N_2 and O_2. N_2 is added to create a stable plasma at equal fractions of CO_2 and CH_4, and because emissions from industrial plants typically contain N_2, while O_2 is added to enhance the process. We test different gas mixing ratios to evaluate the conversion and energy cost. We obtain conversions between 31 and 52 % for CO_2 and between 55 and 99 % for CH_4, with total energy costs between 3.4 and 5.0 eV molecule^{-1}, depending on the gas mixture. This is very competitive when benchmarked with literature. In addition, we present a chemical kinetics model to obtain deeper insight in the underlying plasma chemistry. This allows to determine the major reaction pathways to convert CO_2 and CH_4, in the presence of O_2 and N_2, into CO and H_2. We show that N_2 assists in the CO_2 conversion, but part of the applied energy is also wasted into N_2 excitation. Adding O_2 enhances the CH_4 conversion, and lowers the energy cost, while the CO_2 conversion remains constant, and only slightly drops at the highest O_2 fractions studied, when CH_4 is fully oxidized into CO_2.

Introduction

Global warming is one of today's major environmental problems, and is attributed to enhanced greenhouse gas (GHG) concentrations in the Earth's atmosphere. In this paper we study the combined conversion of CO_2 and CH_4 into CO and H_2, also called "dry reforming of methane" (DRM) [Eq. (1)]:

$$\mathrm{CO_2 + CH_4 \rightarrow 2\,CO + 2\,H_2}$$
$$\Delta H° = +247\ \mathrm{kJ\ mol^{-1}} = +2.6\ \mathrm{eV\ molecule^{-1}} \quad (1)$$

This reaction is highly endothermic and typically carried out at high temperature, raising the energy cost, next to the risk of coking.[1,2]

Several different technologies are being investigated for CO_2 (and CH_4) conversion, such as thermo-, photo-, electro- or bio-chemical conversion, and various combinations, mostly with catalysis.[1,3–5] In this paper, we focus on a different approach, i.e., plasma-chemical conversion. Technologies based on electrical power, such as plasma-chemical but also electrochemical conversion, are very promising, because they can store (excess) renewable electricity in chemical form. Moreover, plasma can easily be switched on/off, making it very promising for peak shaving and grid stabilization.[1]

Plasma is an ionized gas, consisting of various species, including various molecules, radicals, ions, excited species, as well as electrons, which makes it of interest for the conversion of CO_2 and CH_4 because of its high reactivity. The applied electric energy will mainly heat the light electrons, which activate the gas molecules by ionization, excitation and dissociation, leading to various ions, excited species and radicals. The latter easily react further, forming new molecules. Thus, thermodynamically challenging reactions, such as DRM, can proceed at mild conditions of ambient pressure and temperature. Indeed, the gas does not have to be heated as a whole for the reaction to proceed, because the electrons are selectively heated, making the process more energy efficient than classical thermal conversion.[1] Therefore, DRM has been studied in a range of different plasma reactors, with promising results.[1]

In reality, emissions from industrial plants are seldom pure, and they can contain large fractions of N_2. This is not necessarily a problem, and it was even demonstrated in various plasma types that CO_2 splitting can be enhanced upon addition of N_2.[6–8] Moreover, N_2 can help to create a more stable plasma.

Furthermore, the DRM process in plasma was recently found to be positively influenced upon addition of O_2 to the gas mixture.[9–13] This process makes use of partial oxidation of CH_4 [Eq. (2)] to enhance the conversion of CH_4 and simultaneously increase the CO and H_2 production.

$$\mathrm{CH_4 + 1/2\ O_2 \rightarrow CO + 2H_2}$$
$$\Delta H° = -36\ \mathrm{kJ\ mol^{-1}} = -0.37\ \mathrm{eV\ molecule^{-1}} \quad (2)$$

Because of the negative reaction enthalpy, this reaction will occur much easier than DRM. It can make the reforming process very energy efficient and achieve a higher conversion for CH_4. However, undesired side reactions can occur. For example, complete oxidization of CH_4 [Eq. (3)] should be avoided.[9]

$$\mathrm{CH_4 + 2O_2 \rightarrow CO_2 + 2H_2O}$$
$$\Delta H° = -803\ \mathrm{kJ\ mol^{-1}} = -8.3\ \mathrm{eV\ molecule^{-1}} \quad (3)$$

In spite of the interesting results obtained already in literature, [9–13], there is a clear lack in detailed understanding of the process.

In the present paper, we therefore study the conversion of CO_2 and CH_4, in the presence of both N_2 and O_2, in a gliding arc (GA) plasma reactor, more specifically a so-called gliding arc plasmatron (GAP). This reactor was developed at Drexel University by Nunnally et al.[14], to overcome the limitations of classical (two-dimensional) GA reactors, such as limited gas residence time in the arc.

The GAP has previously been tested for gas conversion with promising results for both CO_2 splitting and DRM.[8,14–16] However, no stable plasma could be created for CH_4/CO_2 ratios above 1/4.

Therefore, in the present paper, we add N_2 to create a stable plasma at equal or even larger fractions of CH_4 compared to CO_2. In addition, it was recently demonstrated that N_2 could enhance the CO_2 conversion in the GAP.[8] Furthermore, we also add O_2 in this reactor, to enhance the performance of the DRM process. We will present the conversions, product yields and energy cost of DRM, for different O_2 fractions and CH_4/CO_2 ratios.

In addition, we developed for the first time a comprehensive chemical kinetics model for this complex gas mixture, and we apply it to exactly the same conditions as in the experiments. Subsequently, we use the validated model to explain the experimental data and to provide detailed insight in the chemical composition of the plasma, and in the reaction pathways underlying the conversion process.

Experimental Section

Experimental setup

The GAP reactor is schematically illustrated in Figure 1. It exhibits a sophisticated design, based on tangential inlets, which create an initial vortex that is forced upwards along the reactor wall, which is at cathode potential (green spiral in Figure 1). Once the end of the reactor body (cathode) is reached, the gas travels back in the other direction in a second narrower inner vortex (blue spiral) towards the reactor outlet, which is at anode potential, eventually leaving the reactor. A high voltage is applied between the cathode and the anode, which establishes an initial arc discharge at the shortest distance between the cathode and anode, but the arc is carried with the gas flow until it reaches the end of the cathode. Thus, the arc is positioned along the length of the reactor and stabilized in the middle of the reactor by the inner vortex flow (purple in Figure 1). The use of an inner and outer vortex flow does not only stabilize the arc, but also allows more gas to pass through the arc and creates an isolating effect towards the reactor walls.

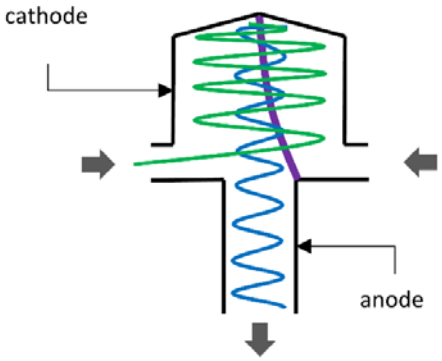

Figure 1. Schematic picture of the GAP reactor with the outer (green) and inner (blue) vortex gas flows, the plasma arc (purple) and electrodes (black). The inlet and outlet in both reactors are indicated with arrows.

A schematic overview of the entire experimental setup, with gas and electrical circuit, is presented in the Supporting Information (SI; Section 1.1, Figure S.1). A schematic cross section of the GAP reactor, with all dimensions indicated, is also given in the SI (Figure S.2).

The gas composition after passing the reactor is measured with a gas chromatograph (GC) (Thermo Scientific trace 1310 GC). A detailed description of the GC measurements is given in the SI (Section 1.1).

We tested the performance of the GAP reactor in a gas mixture of N_2, CO_2, CH_4 and O_2, studying the effect of both CH_4/CO_2 and O_2/CH_4 ratios. An overview of all conditions is given in Table S.1 of the SI. The addition of O_2 to a mixture containing CH_4 could form an explosive mixture, which raises safety concerns. Therefore, every mixture was checked carefully to be out of the explosion regime, as explained in the SI (Section 1.2).

For every condition, we measured the CO_2 and CH_4 conversion and the total conversion, as well as the CO and H_2 yields, with the formulas explained in the SI (Section 1.3), based on the GC measurements with and without plasma. The experiments were performed in triplicate, and for each experiment, four GC measurements were performed, as well as six power measurements and temperature measurements. We took the weighted average of all measurements as the final result for one condition. The SEI and energy cost were determined from the power, flow rate and conversion, as explained by the formulas in the SI (Section 1.3).

Computational part

Besides the experiments, we also developed a zero-dimensional (0D) chemical kinetics model, to obtain a better insight into the plasma chemistry occurring in the GAP reactor. This type of model has no spatial dimensions, as all plasma properties are calculated only as a function of time, hence the name zero-dimensional. However, as the arc forms a column in the middle of the reactor (see Figure 1), which is rather uniform in the radial direction, we can describe it as a plug flow reactor (PFR), i.e., we follow a volume element that flows through the arc, based on the gas flow rate. Due to the equivalence between a PFR (change in gas composition as a function of position) and a batch reactor (change as a function of time), we can translate the temporal evolution of plasma parameters, as calculated in the model, into a spatial evolution, as a function of axial position in the arc, by means of the gas flow velocity, as explained in detail in the SI (Section 2.3). In this way, we obtain a quasi-1D model. This approach is the most suitable for the purpose of this work, as it allows to describe a detailed plasma chemistry without too much computational cost.

We used the Zero-Dimensional Plasma Kinetics solver (ZDPlasKin) to describe the plasma chemistry.[17] It solves the mass conservation equations for all species taken into account in the model, based on production and loss rates, as defined by the chemical reactions. A detailed explanation is given in the SI (Section 2.1).

The initial gas mixture consists of N_2, CO_2, CH_4 and O_2, from which many products can be formed via a wide range of chemical reactions. In total, we included 227 species in our model, i.e., various ions, radicals, excited species and molecules, as well as the electrons. These species are listed in Table S.2 of the SI. The chemistry in the plasma is incorporated by 16210 reaction, i.e., various electron impact reactions, electron-ion recombination reactions, ion-ion, ion-neutral, and neutral-neutral reactions, as well as vibrational-translational (VT) and vibrational-vibrational (VV) relaxation reactions. The latter are important, because we pay special attention to the vibrational levels of the various molecules, which can be important for energy-efficient CO_2 conversion, as will be explained in the Results and Discussion section.

More details on the chemistry, the assumptions made in the model, the input data (such as temperature profile), and the calculation of conversion and yields in the model, both for the gas passing through the arc and outside the arc, can be found in the SI (Section 2).

Results and Discussion

We first present the measured conversions, product yields and energy cost for different gas mixing ratios, and we compare them with the corresponding calculation results. The experiments were always performed in triplicate, but the plasma was very stable, yielding only small error bars, barely visible in the figures. In addition, we also plot the calculated product yields for those products that could not be detected experimentally, e.g., because of their low concentrations. Subsequently, we will provide more detailed modelling results, including analysis of the reaction pathways, for a better understanding of the underlying chemistry.

CO_2 and CH_4 conversion

We tested two different CH_4 fractions, i.e., 10 and 15 %, at a constant CO_2 fraction of 10 %, and we varied the O_2 fraction as much as possible, but taking care to safely stay out of the explosion regime (see details in the SI: Section 1.2). We present the results as a function of both the O_2 fraction and O_2/CH_4 ratio, to allow for easy comparison between the experiments at different CH_4 fractions. The remaining gas fraction is N_2 (between 58.5 and 80 %; see Table S.1 in the SI). The total gas flow rate is kept fixed at 10 L min^{-1}, and the power is between 349 and 472 W (see measurements in SI: Figure S.5).

The measured and calculated CO_2 and CH_4 conversions are plotted in Figure 2. The CO_2 conversion reaches values between 44 and 52 %, nearly independent of the O_2 fraction, except for the 1.1 O_2/CH_4 ratio, which yields a lower CO_2 conversion of 33 and 31 %, for a CH_4 fraction of 10 and 15 %, respectively.

Without O_2 addition, the CH_4 conversion is 62 % for 10 % CH_4 in the mixture, and it slightly drops to 55 %, at 15 % CH_4 in the mixture. Upon O_2 addition, the CH_4 conversion rises dramatically. A maximum conversion of 98 and 99 % is reached for 10 and 15 % CH_4 fraction, respectively, at the highest O_2/CH_4 ratio of 1.1.

This high CH_4 conversion and decreasing CO_2 conversion upon rising O_2 fraction is attributed to the full oxidation of CH_4 due to O_2, producing CO_2, and thus effectively lowering the conversion of the latter. The conversions of CH_4 are significantly higher than those of CO_2, which can be explained by the higher bond strength of the C=O bond in CO_2 (i.e., 5.52 eV vs 4.48 eV for the C-H bond in CH_4),[13] making it more difficult to be converted.

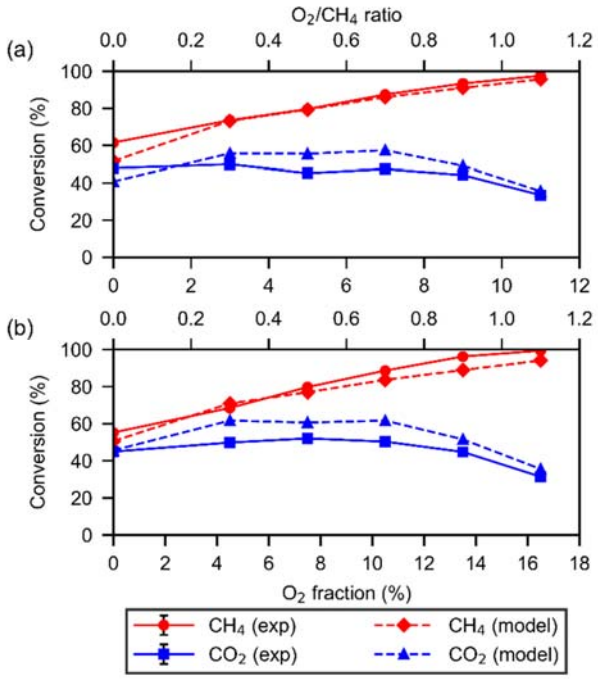

Figure 2. Experimental and modelling results for the CO_2 and CH_4 conversion, as a function of the O_2 fraction and O_2/CH_4 ratio, for a CH_4 fraction of 10 % (a) and 15 % (b). The experiments were performed in triplicate, but the error bars on the experimental results are too small to be visible.

Product yields

The measured and calculated yields for CO and H_2 are depicted in Figure 3; detailed information about the calculations is given in Sections 1.3 and 2.4 of the SI. The CO yield ranges from 8.3 to 13 % for a CH_4 fraction of 10 %, and from 8.2 to 18 % for a CH_4 fraction of 15 %. A higher O_2 fraction enhances the formation of CO, by partial oxidation of CH_4, but for the highest O_2 fractions the yield is reduced again as a result of full oxidation. A higher CH_4 fraction enhances the CO yield for higher O_2 fractions, while it slightly reduces the CO yield when there is no O_2 present. The measured H_2 yield ranges from 6.5 to 9.8 % for 10 % CH_4 and from 10 to 14 % for 15 % CH_4. The O_2 fraction only has a small influence on the H_2 yield, which decreases slightly towards higher O_2 fractions, while a higher CH_4 fraction results in a higher H_2 yield. Besides syngas, a major product detected in our GC is C_2H_2, which reaches its highest yield when no O_2 is present. Its yield decreases from 2.5 to 0.41 % and from 4.6 to 0.40 % upon increasing O_2 fraction, for a mixture with 10 and 15 % CH_4, respectively.

The calculated yields are very close to the experimental values for CO and C_2H_2, but there is a significant deviation for the H_2 yield. Note that the simulations were validated by comparing the CO_2 and CH_4 conversion, but not the product yields. This is an aspect of the model that we should improve in our future research.

It is clear from our model that besides H_2 and CO, H_2O is a major product, but it could not be measured with our GC. Therefore, only the modelling results are displayed in Figure 3, showing a yield ranging from 2.7 to 16 % for 10% CH_4 and from 3.0 to 23 % for 15 % CH_4, i.e., comparable to the CO yield. The strong increase with rising O_2 fraction is due to the full oxidation of CH_4 to CO_2, in which H_2O is produced.

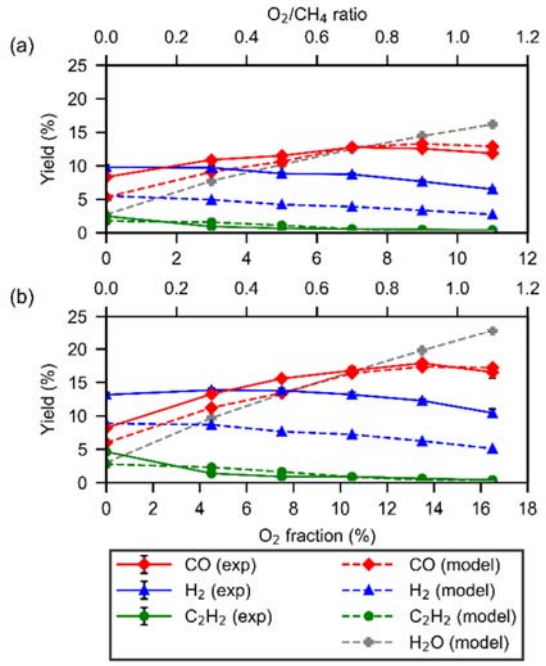

Figure 3. Experimental and modelling results for the CO, H_2 and C_2H_2 yields and modelling results for the H_2O yield, as a function of the O_2 fraction and O_2/CH_4 ratio, for a CH_4 fraction of 10 % (a) and 15 % (b). The yields for CO and C_2H_2 were calculated based on carbon, while the yields of H_2 and H_2O were based on hydrogen. The experiments were performed in triplicate, but the error bars on the experimental results are too small to be visible.

Figure 4 illustrates the calculated yields of the other products that were formed in too small quantities to be detected by our GC. This qualitatively correlates with our modelling results, which indeed predict that they are formed only in minor amounts. It also demonstrates the added value of modelling, to provide extra information that cannot be obtained from the experiments. The C_2H_4, C_2H_6 and C_3H_8 yields, which are the result of CH_4 conversion, reach their maximum when no O_2 is added to the mixture. Indeed, upon O_2 addition, CH_4 is partially converted into oxygenates (including CO and CO_2), and there is less CH_4 left to be converted into hydrocarbons, and thus, the yields of these hydrocarbons decrease upon O_2 addition. The fact that C_2H_2 and C_2H_4 are the major hydrocarbons formed is in agreement with previous studies for DRM in the GAP[15], and it is beneficial, especially for C_2H_4, which is a more valuable product for the chemical industry than e.g., C_2H_6.[18]

The yields of the oxygenates plotted in Figure 4, i.e., CH_2O, CH_3OH and CH_3CHO, follow different trends upon addition of O_2. The CH_2O and CH_3OH yields show a maximum at an O_2/CH_4 ratio of 0.5. This can be explained because both O_2 and CH_4 are needed to form these oxygenates, but at too high O_2 fractions, CH_4 is further oxidized into CO_2, as demonstrated in Figure 2 above. Finally, the H_2O_2 yield increases continuously upon increasing O_2 fraction, as expected.

It is clear from Figures 3 and 4 that DRM in our GAP reactor mainly produces syngas. In our future work, we want to add catalysts after the plasma reactor, to verify whether we can selectively form other compounds in higher amounts, such as light olefins or oxygenates. Note that we added O_2 to enhance the CH_4 conversion, but the O_2 was fully converted into CO (and small fractions of CO_2, for the highest O_2 fractions), and thus no O_2 was left after the reaction. This was found both experimentally, because only trace amounts of O_2 were detected, as well as in our model. This is important, because eliminating O_2 from a syngas mixture is not straightforward, and it would make the downstream processes more expensive.

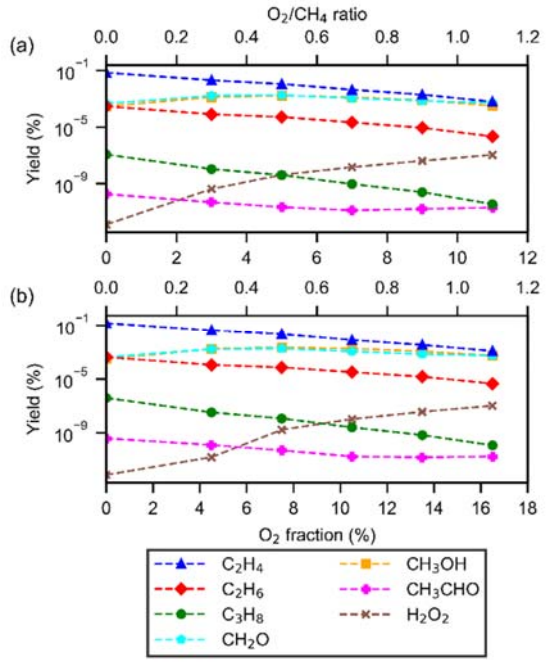

Figure 4. Modelling results for the C_2H_4, C_2H_6, C_3H_8, CH_2O, CH_3OH, CH_3CHO and H_2O_2 yields as a function of the O_2 fraction and O_2/CH_4 ratio, for a CH_4 fraction of 10 % (a) and 15 % (b). The yields for all products plotted in this figure were calculated based on carbon, except for H_2O_2 which was based on hydrogen. The experiments were performed in triplicate, but the error bars on the experimental results are too small to be visible.

Syngas ratio

In Figure 5, we present the measured and calculated syngas ratio, as this is an important parameter for the production of value-added chemicals, such as fuels or methanol. Our measured H_2/CO ratio varies from 1.19 to 0.56 upon increasing O_2 fraction, for the gas mixture with 10 % CH_4, and from 1.72 to 0.63 for the gas mixture with 15 % CH_4, while our calculated values are somewhat lower. This is attributed to the H_2 production that is slightly underestimated in our model. The addition of O_2 significantly reduces the H_2/CO ratio, due to the formation of more H_2O and oxygenates, as seen in Figures 3 – 4 above.

Thus, our obtained syngas ratio is quite lower than the ideal syngas ratio for practical Fischer-Tropsch synthesis, which is typically between 1.7 and 2.15, depending on the catalyst and operating conditions.[19] When using it for methanol synthesis, the syngas ratio needs to be even higher, i.e., up to 3, which could not be reached in our experiments. However, some special catalysts can produce alcohols from a lower syngas ratio of 1.[19] We believe a more suitable syngas ratio could be reached when increasing the CH_4 fraction in the mixture. This is planned for our future work.

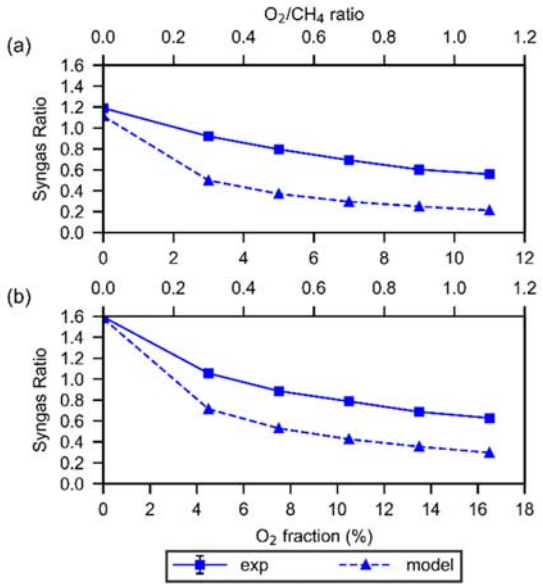

Figure 5. Experimental and modelling results for the syngas ratio (H_2/CO), as a function of the O_2 fraction and O_2/CH_4 ratio, for a CH_4 fraction of 10 % (a) and 15 % (b). The experiments were performed in triplicate, but the error bars on the experimental results are too small to be visible.

Energy cost of the conversion

The energy cost is obtained from the total conversion and the specific energy input (SEI); see formulas in the SI (Section 1.3). The total conversion is calculated as the sum of the individual conversions of CO_2 and CH_4, each multiplied with their fraction in the mixture, and is plotted in SI Figure S.4. The SEI is defined by the ratio of plasma power over gas flow rate. Both the plasma power and SEI are also plotted in the SI (Figures S.5 and S.6), as a function of O_2 fraction and O_2/CH_4 ratio. The power ranges between 349 and 472 W for the different conditions (see measurements in SI: Figure S.5). Because we use a constant gas flow rate of 10 L min^{-1} in these experiments, the SEI varies around 2.1 – 2.8 kJ L^{-1} (or 0.5 – 0.7 eV $molecule^{-1}$). The resulting energy cost is plotted in Figure 6 for the various conditions investigated. We plot the results both in eV $molecule^{-1}$ (left y-axis) and in kJ L^{-1} (right y-axis), because the first one is most relevant to benchmark our results with other plasma processes, while the latter one is more relevant for process chemistry.

An energy cost of 19.7 kJ L^{-1} (or 5 eV $molecule^{-1}$) is reached for mixtures without O_2 and a fraction of 10 % CH_4. A higher CH_4 fraction of 15 % slightly increases the energy cost to 21 kJ L^{-1} (or 5.34 eV $molecule^{-1}$), which is logical, because of the higher power needed to establish the plasma (see SI Figure S.5). When adding O_2 to the gas mixture, the energy cost decreases, reaching a minimum of 15.9 and 13.4 kJ L^{-1} (corresponding to 4.03 and 3.39 eV $molecule^{-1}$) for 10 and 15 % CH_4 in the mixture, respectively, at an O_2/CH_4 ratio of 0.9. The higher O_2/CH_4 ratio of 1.1 shows a somewhat higher energy cost of 16.0 and 13.5 kJ L^{-1} (or 4.06 and 3.43 eV $molecule^{-1}$), for the two CH_4 fractions, due to the slightly lower total conversion (see SI Figure S.4).

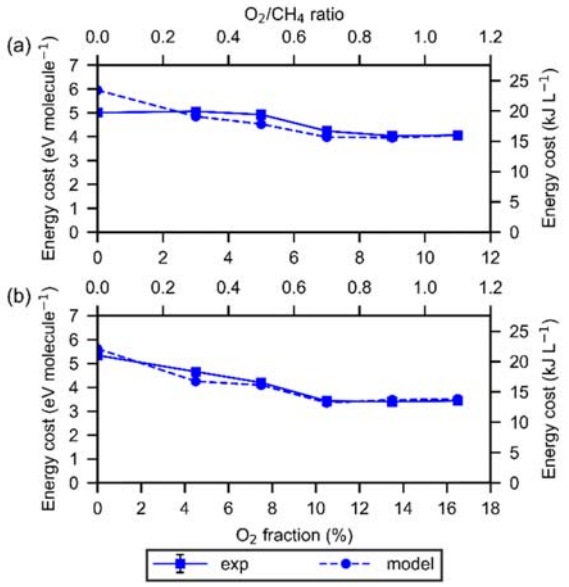

Figure 6. Experimental and modelling results for the energy cost of the total CO_2 and CH_4 conversion, as a function of the O_2 fraction and O_2/CH_4 ratio, for a CH_4 fraction of 10 % (a) and 15 % (b). The experiments were performed in triplicate, but the error bars on the experimental results are too small to be visible.

Our results indicate that the gas mixture with 15 % CH_4, and either 10.5 or 13.5 % O_2 (corresponding to an O_2/CH_4 ratio of 0.7 or 0.9) yields the lowest energy cost, in combination with a high conversion of CH_4, without losing CO_2 conversion. An O_2 fraction of 16.5 % also yields a low energy cost and even a slightly higher CH_4 conversion (near 100 %). However, the CO_2 conversion is lower in this case, due to the full oxidation of CH_4, producing CO_2, as explained above. Higher O_2 fractions were not possible, because of risks to enter the explosion regime, and they would not give a further enhancement in CH_4 conversion, which is already near 100 %, while they would further reduce the CO_2 conversion. Higher CH_4 fractions were not possible either, again because of risks to enter the explosion regime, as well as due to coking issues. These values of conversion and energy cost will be benchmarked below with literature data.

Note that our definition of energy cost does not account for heat recovery, and for the energy needed to run the reactor. Indeed, we use the plasma power as input, to allow benchmarking with other plasma processes, where this is standard practice, in order to identify the efficiency of the plasma process itself. However, to define the real energy cost, we would need to consider the power from the wall socket. For our GAP reactor, we measured the ratio between plasma power and applied power, and obtained roughly an efficiency of 75 – 80 %, so it means that the actual energy cost, when accounting for the efficiency of the power supply, would be a factor 1.3 higher. In addition, we don't take into account the cost of product separation, which would also add to the overall cost of the process. On the other hand, if we would be able to include heat recovery, this could reduce the overall energy cost, because our GAP reactor operates at a temperature around 1500 – 3000 K. We would like to investigate this in our future work.

Temperature of the gas leaving the reactor

We recorded the temperature of the gas leaving the GAP reactor with a thermocouple at a distance of 26 cm from the GAP outlet (see details in the SI, Section 1.1). This temperature rapidly increases after igniting the plasma but stabilizes after some time. Therefore, we started the filling of the sample loops in the GC only after 10 min, to let the temperature and plasma stabilize. The observed temperature at the start and the end of the filling of the sample loops in the GC is displayed in Figure 7. It is clear that the temperature still rises during the filling of the sample loops, meaning that the plasma was not yet fully stabilized, but this was not reflected in the GC measurements (cf. the very small error bars in our obtained conversions, yields and energy costs; see Figures 2 – 4, 6, and SI). In addition, the temperature rises with increasing O_2 fraction, which is like expected, as the partial and full oxidation of CH_4 are both exothermic reactions. Without O_2, the temperature is around 150 °C, and it rises to above 300 °C for O_2/CH_4 ratio of 1.1. Increasing the CH_4 fraction from 10 to 15 % shows only a minor influence on the temperature.

It should be noted that these values do not represent the plasma temperature, which is in the order of 2000-3000 K[20] (see also SI Figure S.3), and thus, also the temperature directly flowing out of the GAP will be higher, but it could not be measured in the experimental setup (see SI Figure S.1). However, the temperature values in Figure 7 give an indication of the influence of the gas mixture on the temperature in the reactor as well. In addition, in future research, we would like to combine the GAP with post-plasma catalysis, so it will be interesting to measure the temperature as closely as possible to the GAP outlet, and at varying

positions from the outlet, to determine the optimal position of a catalyst bed. Indeed, the temperature values presented in Figure 7 indicate that heat recovery of the plasma for catalyst activation could be a viable option.

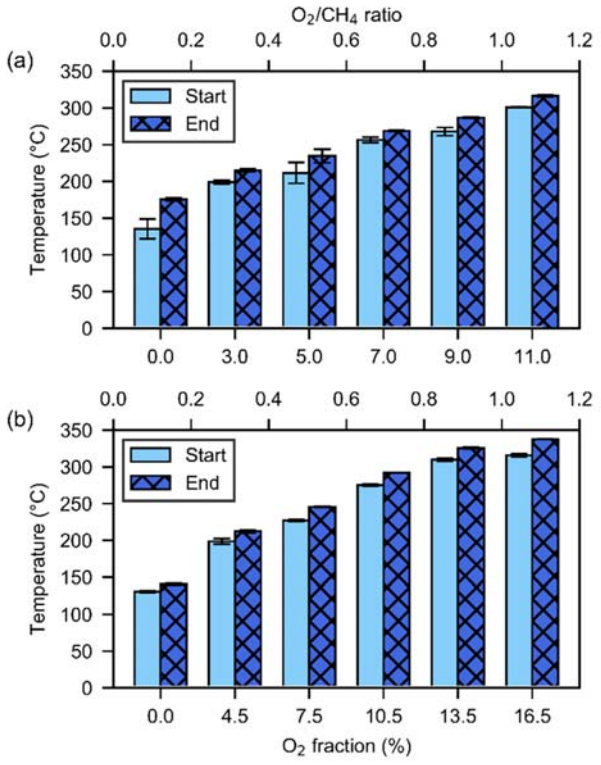

Figure 7. Temperature of the exhaust gas flow, as a function of the O_2 fraction and O_2/CH_4 ratio, at the start and the end of the filling process of the GC sample loops, for a CH_4 fraction of 10 % (a) and 15 % (b).

Benchmarking of our results with other research

To benchmark our results with the available literature, we compare in Table 1 our CO_2 and CH_4 conversions, energy cost and H_2/CO ratios, obtained in this gas mixture (N_2, CH_4, CO_2 and O_2), to other plasma-based DRM results in literature, i.e., those obtained previously in the same GAP reactor for DRM, but without N_2 and O_2 addition (in which only CH_4/CO_2 ratios up to a maximum of 1/4 were possible)[15], as well as with other plasma reactor types from literature.[9,12,21,22] Our results yield the highest CH_4 conversion of all the available results.

When looking at the GAP reactor, it is clear that DRM without additional gases achieved much lower conversions for both CH_4 and CO_2,[15] i.e., about half of what we could achieve in our work. On the other hand, the energy cost was lower than for our results. This is attributed to the overall gas mixture, only consisting of CO_2 and CH_4, where no energy had to be put into O_2 and N_2. Indeed, N_2 assists in the CO_2 conversion, as mentioned in the Introduction, and also explained below, but part of the applied electric power is also wasted into excitation and ionization of N_2, and can therefore not all be used for CO_2 and CH_4 conversion. This indicates that if the fraction of N_2 in our mixture could be reduced, while still maintaining a stable plasma, we expect to reach lower energy costs. This will be investigated in future work.

The results of the AC pulsed GA reactor show a similar trend, i.e., for the same $CH_4/CO_2/O_2$ ratio, a much lower energy cost was obtained without N_2 present.[9] For this reactor, lower conversions were obtained than in our work, but an exact comparison cannot be made, due to the different gas fractions and different flow rate used. The spark discharge plasma obtained a higher CO_2 conversion but lower CH_4 conversion, albeit at a low flow rate.[12] While achieving this high CO_2 conversion, the energy cost is almost twice as high compared to our results.

The DBD plasma shows similar CO_2 conversion but lower CH_4 conversion compared to our results, and a significantly higher energy cost (551 kJ L^{-1}) was obtained at a very low flow rate.[21] The microwave plasma shows the highest CO_2 conversion, but a lower CH_4 conversion, and the energy cost is almost twice as high as for our results.[22]

The reason why the energy cost in our study is quite low, especially compared to the DBD results, is attributed to the significant populations of the vibrational excitation levels of CO_2, as demonstrated in the SI (Figure S.19). Indeed, the reduced electric field (i.e., ratio of electric field over gas number density: E/n) in a GA plasma (as well as in MW plasmas) is in the order of 50 Td, and this provides the right electron energy for predominant vibrational excitation of CO_2 molecules, which is the most efficient CO_2 dissociation pathway,[1] while a DBD is typically characterized by a reduced electric field above 200 Td, causing more electronic

excitation and ionization, which require more energy than strictly needed for dissociation, meaning a waste of energy, and thus a higher energy cost.[1]

Figure S.7 in the SI provides an overview of energy cost vs total conversion for DRM, for a wide range of different plasma types.[1] Our results are added to this figure, with red dots. They lie in the upper half of the GA results, with energy cost lower than the thermal conversion line, and even below the line of the efficiency target, defined in Snoeckx et al.[1] as a target for plasma to be competitive with other (existing or emerging) technologies. In other words, this is an improvement over thermal conversion, and even better than the defined efficiency target.[1] Of course, it must be realized that some O_2 is added here, which makes the overall reaction less endothermic, and it enhances the CH_4 conversion, thus lowering the energy cost.

The total conversion reached in our work is however still only about 20 %, which is in the lower half of the GA results, and lower than for many other plasma reactors. Nevertheless, we believe this could be improved if we can reduce the N_2 fractions in the mixture, while still maintaining a stable plasma, because the latter limits the effective CO_2 and CH_4 conversions (because of their limited fractions in the mixture) and thus the total conversion.

Table 1. Overview of operating conditions (gas mixture, flow rate, power) and results for DRM (CO_2 and CH_4 conversion, energy cost, syngas ratio) for different plasma reactor types, as well as for conventional DRM.

Reactor type	Gas mixture	Flow rate (L min^{-1})	Power (W)	CO_2 conversion (%)	CH_4 conversion (%)	Energy cost (kJ/L (eV $molecule^{-1}$))	H_2/CO ratio	Ref.
GAP	CH_4, CO_2, O_2, N_2 (10 %, 10 %, 9 %, 71 %)	10	364	44	93	15.9 (4.0)	0.60	This work
GAP	CH_4, CO_2, O_2, N_2 (15 %, 10 %, 13.5 %, 61.5 %)	10	421	45	96	13.4 (3.4)	0.68	This work
GAP	CH_4, CO_2 (25 %, 75 %)	10	531	23	41	11.4 (2.9)	0.44	[15]
AC pulsed GA[a]	CH_4, CO_2, O_2, N_2 (22 %, 15 %, 13 %, 50 %)	15	280	25	77	5.4[a] (1.4)	-	[9]
AC pulsed GA[a]	CH_4, CO_2, O_2 (44 %, 29 %, 27 %)	15	280	27	81	2.6[a] (0.65)	1[d]	[9]
Spark discharge[b]	CH_4, CO_2, O_2 (53 %, 35 %, 12 %)	0.2	64	67	80	29.3[b] (7.4)	1.5[d]	[12]
DBD	CH_4, CO_2 (50 %, 50 %)	0.02	107	44	73	551[c] (140)	-	[21]
MW	CH_4, CO_2 (60 %, 40 %)	0.2	60	69	71	25.6 (6.5)	1.5	[22]
Thermal DRM	CH_4, CO_2 (50 %, 50 %)	0.1	-	75	68	-	0.87	[23]

[a] The energy cost for the formation of CO + H_2 was provided – we list here the value calculated in the same way as for our results. [b] The energy cost for the formation of H_2 was provided – we list here the value calculated in the same way as for our results. [c] No energy cost was provided – we list here the value calculated from their results in the same way as for our results. [d] Deduced from the graphical results in this paper.

It should be noted that comparison with literature data must be made with caution, because many papers in literature do not account for the gas expansion factor when calculating their conversions and energy costs, or at least there is no indication whether the gas expansion factor was employed, so most probably it was not accounted for. In the SI (Figures S.8 – S.10), we illustrate that this can affect the results, by overestimating the conversion and underestimating the energy cost. The effect is not so pronounced in our case, because we use a large excess of N_2, but it can be very dramatic when using a pure CO_2/CH_4 mixture (without O_2 or N_2 addition), as explained in the SI.

In general, we can conclude that the addition of O_2 (and to some extent N_2) to the gas mixture has a beneficial effect on DRM in the GAP, which shows competitive results compared to other gas mixtures and other types of plasma reactors.

Table 1 also shows the range of H_2/CO ratios obtained in the various plasma processes from literature, in comparison with our results. Our results yield a higher syngas ratio than previous results from the GAP, while the results obtained in an AC pulsed GA yielded a syngas ratio of 1, and in a spark discharge and MW plasma reactor, a syngas ratio of 1.5 was reached, which is more beneficial for the Fischer-Tropsch process. These results were however obtained for an inlet mixture with a low O_2 fraction or even without O_2 in the case of the MW reactor, thus forming less oxygenates and less H_2O, explaining the higher syngas ratio. In our reactor we also reached a ratio of up to 1.6 without O_2 present.

Finally, we compare our results with conventional DRM (see last row in Table 1, showing results for a Ni-based catalyst). It should however be noted that a wide range of catalytic materials is being used for DRM, so comparing with just one catalyst might not be fully representative. Nevertheless, we can conclude that the CO_2 conversion is much lower in our plasma reactor, but we achieve a higher CH_4 conversion. The syngas ratio is slightly higher for this catalyst compared to our results, but still lower than ideal for Fischer-Tropsch synthesis. Unfortunately, we could not directly compare the energy cost of conventional DRM with our results. However, Snoeckx and Bogaerts.[1] defined an efficiency target for the energy cost of 4.27 eV/molecule (which corresponds to 16.8 kJ/L) for pure plasma-based DRM to be economically viable. We can conclude that our reactor can reach this target value. The energy cost also decreases with increasing CH_4 fraction, and this could also help further improve the energy cost in the future.

As shown in previous sections, the measured conversions, H_2 and CO product yields, and energy costs were in good agreement with the calculated data, obtained with our model that we developed for this purpose, both in absolute values, as well as in the behaviour as a function of gas mixing ratios, for all gas mixtures investigated. It should be mentioned that we slightly adjusted the temperature profile, used as input in the calculations, as explained in detail in the SI (Section 2.3), but we did not use any other fitting parameters. Thus, our model can provide a realistic picture of the plasma chemistry, and we can use it to obtain more insight in the underlying mechanisms. Indeed, the model can provide more information, apart from the conversions, product yields and energy cost, beyond what is possible to measure experimentally, and thus, it is extremely valuable to obtain more detailed insight in the process. In the following sections, we will discuss the contribution of the conversion inside and outside the arc region, as

well as the populations of the CO_2 vibrational levels (crucial for energy-efficient CO_2 dissociation), both inside and outside the arc. In addition, we will elucidate the underlying mechanisms and reaction pathways to convert CO_2, CH_4 and O_2 into CO and H_2, along with the important intermediate products.

Calculated conversion inside and outside the arc region

The modelling results in Figures 2 – 4 show similar values as the experimental data, which is quite impressive, in view of the complexity of the underlying plasma chemistry included in this model. However, we found that when our model only covers the arc region in the reactor, no good agreement could be reached with the measured conversions. Indeed, we had to perform additional simulations outside (but near) the arc, as explained in the SI (Section 2.3 and 2.4), to account for thermal conversion in this region. The combination of these two simulations provides a better approximation of the reality and a better agreement with the experimental results, as shown in detail in the SI (Figures S.11 and S.12) for both CO_2 and CH_4 conversion. Indeed, our simulations indicate that for all gas mixtures investigated, a large fraction of CO_2 and nearly all CH_4 in the arc is converted (see below). However, this results in only 13.8 % of the overall conversion being achieved in the arc, because the latter is limited by the fraction of gas passing through the arc, obtained from 3D fluid dynamics simulations.[20] Thus, a large fraction of CO_2 and CH_4 is not passing through the arc, but is still converted by thermal reactions. In other words, the conversion outside the arc accounts for a larger part of the total conversion, as a result of the much larger fraction of gas that is not passing through the arc.[15,20]
Figures S.13 and S.14 plot the calculated density profiles of CO_2 and CH_4, as well as of the major products, CO and H_2, as a function of position in the reactor, both inside the arc and in the region around the arc. It is clear that CO_2 and CH_4 are almost immediately converted into CO and H_2 in the beginning of the arc column, illustrating that most of the reactions occur in the first micrometres of the arc and then reach a steady state, as the forward and reverse reactions become comparable.

Calculated vibrational distribution function (VDF) of CO_2

Figures S.11 and S.12 in the SI illustrate that CH_4 and CO_2 are partially converted both inside and outside the arc. For CH_4, this is largely due to thermal reactions, with additional contributions of plasma-chemical reactions (induced by electrons) inside the arc, as will be explained below. However, for CO_2, the underlying processes are different, and can be explained by the vibrational excitation of CO_2. Indeed, as indicated in the Introduction and in the benchmarking above, a GA plasma exhibits quite low energy costs, in comparison to other plasma reactors (especially DBD plasmas), and this is attributed to higher populations of the vibrational excitation levels of CO_2. Especially the asymmetric stretch mode is important for energy-efficient CO_2 dissociation,[1] and therefore, our model includes all asymmetric mode levels up to the dissociation limit, i.e., 21 levels in total (see details in the SI, Section 2.2), besides four symmetric mode levels, as explained in Kozák et al.[24]
Figure S.19 in the SI illustrates the calculated normalized densities of these 4 symmetric and 21 asymmetric vibrational mode levels, i.e., so-called vibrational distribution function (VDF), as well as of the ground state of CO_2, at the end of the reactor, both inside the plasma arc and in the area around it, in comparison with the Boltzmann VDF.
Inside the arc we observe an increased population of the higher vibrational levels, relative to the Boltzmann distribution, which is beneficial for energy-efficient CO_2 splitting. This can be explained as follows: The lower vibrational levels are populated by electron impact vibrational excitation, which is a very efficient process in the GA, because the electrons have the right energy for this process, as discussed above. Subsequently, the higher vibrational levels of CO_2 are gradually populated upon collision with other vibrational levels, in so-called vibrational-vibrational (VV) relaxation reactions. This so-called ladder climbing process proceeds up to the highest levels, with excitation energy around 5.5 eV, which easily dissociate into CO and O atoms, because this energy corresponds to the C=O bond dissociation energy. This vibrational pathway makes the CO_2 dissociation inside the arc quite energy-efficient and can explain the low energy costs obtained in our GAP reactor (cf. Figure 6). Outside the arc, the VDF exhibits no enhancement compared to the Boltzmann distribution, as is clear from Figure S.19, which points towards thermal CO_2 dissociation and the absence of the ladder climbing process.

Reaction pathway analysis of the conversion of CO_2, CH_4 and O_2 into CO and H_2

The main objective for the model is to analyse the underlying chemistry of the conversion of CO_2, CH_4 and O_2 into CO and H_2, to better understand the mechanisms, and thus to support the experiments to further improve the performance. We only focus on the reactions inside the arc, and not in the area around the arc, which does not contain electrons, and is simply characterized by thermal conversion. The detailed analysis, based on comparing the average reaction rates throughout the plasma arc of the different reactions involved for the species under study, is presented in the SI (Section 3.9).
Based on this detailed reaction analysis, we can obtain insight in the important reaction pathways for the conversion of CO_2 and CH_4 in the presence of O_2 and N_2. We show this analysis again for the intermediate gas mixture of 73 % N_2, 10 % CO_2, 10 % CH_4 and 7 % O_2. The pathway scheme is given in Figure 8. This is of course a simplified description of the entire chemistry occurring in the plasma.
As discussed in previous section, CO_2 is first vibrationally excited via electron impact collisions, as well as collisions with neutral species (M) or VV relaxations, to the lowest vibrational levels ($CO_2(V_1)$). This is followed by VV relaxations to populate the higher vibrational levels ($CO_2(V_{>1})$). Besides the asymmetric mode levels of $CO_2(V_{1\text{-}21})$, also the symmetric mode vibrational levels ($CO_2(V_{a\text{-}}$

$_d$)) are populated in this manner. The VV relaxations can occur upon collision with any vibrationally excited species, but in the mixture under study, the vibrational levels of N_2 and CO are the most involved in this process for the asymmetric mode vibrational levels, while the symmetric mode levels are mostly populated by VV reactions with other CO_2 molecules. Indeed, the major role of N_2 in the mixture, besides stabilizing the plasma, as explained above, so that larger CH_4 fractions can be considered in the mixture,[15] is to assist in this process of vibrational ladder climbing. Note that its dissociation into N atoms, from which other N-compounds (e.g., NOx, NH, NHO, …) can be formed, is found to be of minor importance at the conditions under study. Therefore, only N_2, $N_2(V_1)$ and $N_2(V_{>1})$, but no other N-compounds are shown in the diagram of Figure 8. For both CO_2 and N_2, the higher vibrational levels can also relax back to lower levels, by either VV or VT (vibrational-translational) relaxations. The latter process is generally more important at higher gas temperature, and should be avoided, as it reduces the energy efficiency of the conversion process. It is therefore important to have a strong non-equilibrium between the vibrational and translational (gas) temperature in the plasma.

After CO_2 has reached high enough vibrational energy, it dissociates through reaction with either H [Eq. (4)] or a neutral plasma species [Eq. (5)].

$$CO_2(V) + H \rightarrow CO + OH \quad (4)$$

$$CO_2(V) + M \rightarrow CO + O + M \quad (5)$$

The lower vibrational levels ($V_{<14}$) react mostly through Equation (4), while the higher vibrational levels ($V_{\geq 14}$) react almost exclusively through Equation (5), in which M is mostly N_2, because of its highest fraction in the mixture.

In parallel, O and OH are also produced in the plasma, from the added O_2 in the mixture, through the reaction in Equation (6), which is the most important O_2 loss process.

$$O_2 + H \rightarrow O + OH \quad (6)$$

The produced O atoms react with H_2 [Eq. (7)] and CH_4 [Eq. (8)] into OH.

$$H_2 + O \rightarrow OH + H \quad (7)$$

$$CH_4 + O \rightarrow CH_3 + OH \quad (8)$$

The formed OH can react with several species, such as $H_2(V_1)$ [Eq. (9)], CH_4 [Eq. (10)], C_2H_2 [Eq. (11)], OH [Eq. (12)] and CH_3 [Eq. (13)] to form H_2O.

$$OH + H_2(V_1) \rightarrow H_2O + H \quad (9)$$

$$OH + CH_4 \rightarrow H_2O + CH_3 \quad (10)$$

$$OH + C_2H_2 \rightarrow H_2O + C_2H \quad (11)$$

$$OH + OH \rightarrow H_2O + O \quad (12)$$

$$OH + CH_3 \rightarrow H_2O + CH_2 \quad (13)$$

The H atoms, produced in Equations (7) and (9), react with H_2O to H_2, following Equation (14).

$$H + H_2O \rightarrow H_2 + OH \quad (14)$$

Importantly, the OH radicals do not only contribute to the H_2O and H_2 production, but also to the loss of CO, which will partially react back to CO_2 (see Equation (15), and thick arrow line in the upper part of the diagram).

$$CO + OH \rightarrow CO_2 + H \quad (15)$$

The above reactions summarize how CO_2 is converted and how CO and H_2 are formed, as well as how O_2 and N_2 are involved in these pathways. In addition, CH_4 is converted in some reactions involving OH, but these are only partially responsible for the CH_4 conversion. Indeed, CH_4 is mainly split into H and CH_3 by thermal reactions with various molecules (M), mostly N_2, H_2 and H_2O. Vice versa, CH_3 and H can also recombine back into CH_4 in three-body collisions with multiple species as third body, e.g., N_2 and H_2O, as indicated in Figure S.23 of the SI.

In addition, the H atoms formed from CH_4 splitting also react with O_2 and $CO_2(V)$ into O and OH, which cascade towards H_2O and H_2 as described above. Next to the H atoms, the CH_3 radicals are a major product formed from CH_4 splitting, and they can react further into a range of different species, such as C_2H_2, C_2H_4, CH_2O, CH_3OH, … However, because the latter are only formed in low quantities (cf. Figures 3 and 4), they are not displayed in the pathways of Figure 8.

It should be noted that the pathways drawn in Figure 8 apply to the specific gas mixture of 73 % N_2, 10 % CO_2, 10 % CH_4 and 7 % O_2. Changing the O_2 fraction affects the chemistry, as discussed above, and this will be reflected in the pathways. However, for all O_2 fractions investigated, the changes are only in relative size of the arrows, while the pathways themselves are the same. On the other hand, without O_2 some differences are observed in the pathways. The H atoms obtained from CH_4 splitting will not react (so much) with O_2 as there is less O_2 present (only some fraction produced from CO_2 splitting). Therefore, the reverse reaction is much more important in this case, leading to a lower CH_4 conversion, as indeed observed in the experiments (cf. Figure 2). In addition, the reaction between H and O_2 will be less important, because the O_2 present only originates from CO_2 splitting, so there is less OH being produced, which also leads to a lower reverse reaction from CO to CO_2. There is still some production of OH and H_2O, as CO_2 is still converted in O atoms that can form OH and H_2O, but only in much lower quantities. This also explains why the conversion of CH_4 increases and the conversion of CO_2 decreases at 11 % O_2 fraction. The amount of O_2 in the mixture is then higher than that of CH_4, and it will quickly consume the produced H atoms from CH_4 splitting, resulting in high OH amounts, which convert CO back into CO_2, effectively decreasing its conversion. A similar behaviour was reported upon H_2O addition to a DBD plasma operating in CO_2.[25]

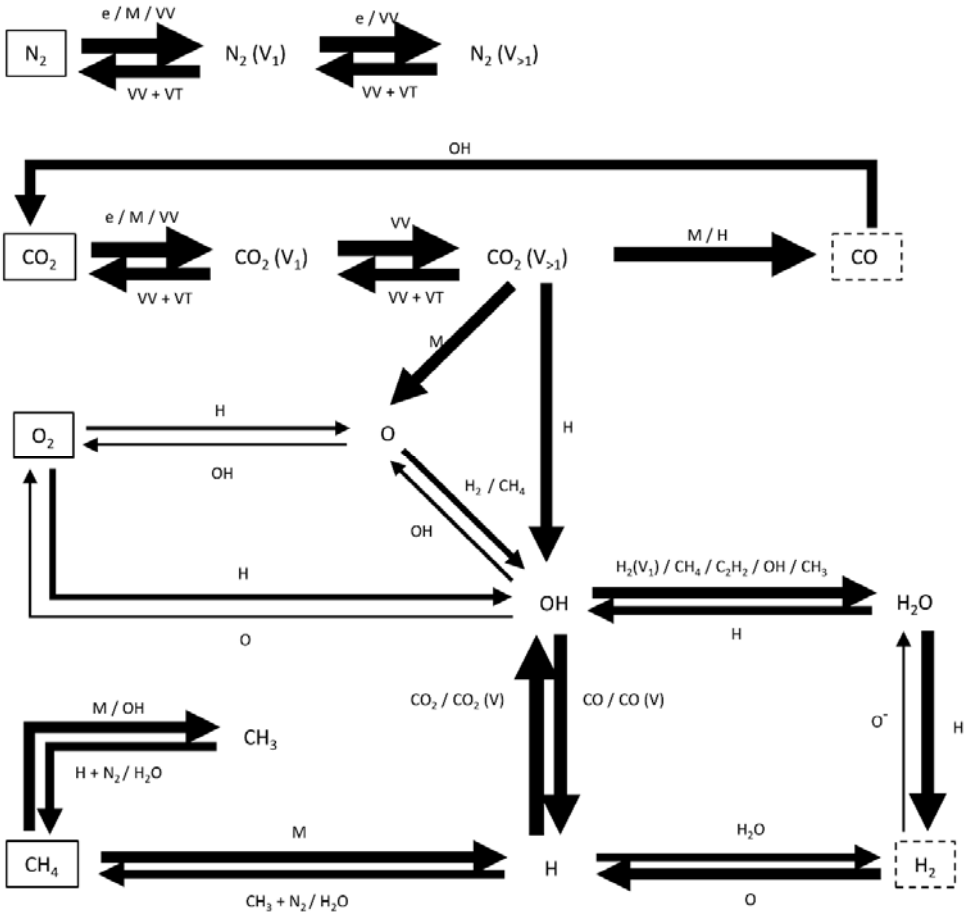

Figure 8. Main reaction pathways for the conversion of CO_2, CH_4 and O_2 into CO and H_2, through various intermediate species, as determined from the simulations with 73 % N_2, 10 % CO_2, 10 % CH_4 and 7 % O_2 inside the arc. The thickness of the arrow lines indicates the importance of the reactions. See details in SI (Figures S.20 – S.27).

Conclusions

In this paper, we investigated the conversion of CH_4 and CO_2 into CO and H_2 in a GAP, upon addition of O_2 and N_2 to the mixture, showing promising results for DRM. O_2 addition results in a higher CH_4 conversion, while the CO_2 conversion was only slightly reduced upon adding high O_2 fractions. The CO and H_2 yields were also determined: the CO yield rises upon addition of O_2, while the H_2 yield slightly decreases. The energy cost also drops with increasing O_2 fraction, which is interesting for future applications from an economical point of view. Using an O_2 fraction larger than the CH_4 fraction, however, results in a lower CO_2 conversion, because CH_4 is fully oxidized into CO_2, thus reducing the net CO_2 conversion. This also increases the energy cost. The best results were obtained for a high O_2 and CH_4 fraction, i.e., a mixture of 61.5 % N_2, 15 % CH_4, 10 % CO_2 and 13.5 % O_2. At these conditions, the CO_2 and CH_4 conversion reached 44 and 96 %, respectively, yielding an energy cost of 13.4 kJ/L or 3.4 eV molecule^{-1}. The benefit of adding O_2 to the mixture, i.e., to increase the CH_4 conversion and to reduce the energy cost, is slightly outweighed by the drop in H_2/CO ratio of the produced syngas. The results can possibly be further enhanced by a change in the reactor design, to allow more gas passing through the arc plasma. This is especially important for improving the CO_2 conversion, because the CH_4 conversion largely proceeds by thermal reactions, so it also occurs in the hot region around the arc plasma.

Next to experiments, we also performed simulations for the different conditions studied experimentally. These simulations allow to obtain insight in the plasma chemistry, and to reveal the underlying reaction pathways. The overall conversion was obtained as the combination of conversion in the plasma arc and thermal conversion in the area around the arc. Inside the arc, both CO_2 and CH_4 can reach high conversions, but as the fraction of gas passing through the arc is limited, the thermal conversion outside the arc proved to be very important in the overall CO_2 and CH_4 conversion. The reaction pathways elucidated in this study confirm the ladder climbing process for the conversion of CO_2 and how this ties into the rest of the plasma chemistry. The H and OH radicals

were found to be important in the mechanism to convert CO back into CO_2, and this lowers the CO_2 conversion, which is influenced by the O_2 fraction present in the gas mixture.
In general, our work illustrates that the addition of O_2 to the DRM gas mixture greatly improves the results. When benchmarking our results with the available literature, we obtain the highest CH_4 conversion, and a very competitive energy cost, when compared to other types of plasma reactors.
Adding N_2 was needed to create a stable plasma, and it also mimics emissions from industrial plants. In addition, N_2 is found to assist in the CO_2 conversion, but part of the applied electric power is also wasted into excitation and ionization of N_2 and can therefore not all be used for CO_2 and CH_4 conversion. This indicates that if the fraction of N_2 in our mixture could be reduced, we expect to reach lower energy costs. This will be investigated in future work.

Conflicts of interest

There are no conflicts to declare.

Acknowledgements

We acknowledge financial support from the European Research Council (ERC) under the European Union's Horizon 2020 research and innovation programme (grant agreement No 810182 – SCOPE ERC Synergy project), the Excellence of Science FWO-FNRS project (FWO grant ID GoF9618n, EOS ID 30505023), and the FWO postdoctoral fellowship of M. A. (Grant number 12M7118N). This work was carried out in part using the Turing HPC infrastructure at the CalcUA core facility of the Universiteit Antwerpen, a division of the Flemish Supercomputer Center VSC, funded by the Hercules Foundation, the Flemish Government (department EWI) and the University of Antwerp.

Notes and references

1 R. Snoeckx and A. Bogaerts, *Chem. Soc. Rev.*, 2017, **46**, 5805–5863.
2 M. Scapinello, E. Delikonstantis and G. D. Stefanidis, *Chem. Eng. Process: Process Intensif.*, 2017, **117**, 120–140.
3 F. A. Rahman, M. M. A. Aziz, R. Saidur, W. A. W. A. Bakar, M. . Hainin, R. Putrajaya and N. A. Hassan, *Renewable. Sustainable. Energy Rev.*, 2017, **71**, 112–126.
4 G. Centi and S. Perathoner, *Catal. Today*, 2009, **148**, 191–205.
5 B. Hu, C. Guild and S. L. Suib, *J. CO2 Util.*, 2013, **1**, 18–27.
6 S. Heijkers, R. Snoeckx, T. Kozák, T. Silva, T. Godfroid, N. Britun, R. Snyders and A. Bogaerts, *J. Phys. Chem. C*, 2015, **119**, 12815–12828.
7 R. Snoeckx, S. Heijkers, K. Van Wesenbeeck, S. Lenaerts and A. Bogaerts, *Energy Environ. Sci.*, 2016, **9**, 999–1011.
8 M. Ramakers, S. Heijkers, T. Tytgat, S. Lenaerts and A. Bogaerts, *J. CO2 Util.*, 2019, **33**, 121–130.
9 J.-L. Liu, H.-W. Park, W.-J. Chung, W.-S. Ahn and D.-W. Park, *Chem. Eng. J.*, 2016, **285**, 243–251.
10 P. Thanompongchart, P. Khongkrapan and N. Tippayawong, *Period. Polytech. Chem. Eng.*, 2014, **58**, 31.
11 N. Rueangjitt, T. Sreethawong and S. Chavadej, *Plasma Chem. Plasma Process.*, 2008, **28**, 49–67.
12 B. Zhu, X.-S. Li, J.-L. Liu and A.-M. Zhu, *Int. J. Hydrogen Energy*, 2012, **37**, 16916–16924.
13 X. Zhu, K. Li, J.-L. Liu, X.-S. Li and A.-M. Zhu, *Int. J. Hydrogen Energy*, 2014, **39**, 13902–13908.
14 T. Nunnally, K. Gutsol, A. Rabinovich, A. Fridman, A. Gutsol and A. Kemoun, *J. Phys. D. Appl. Phys.*, 2011, **44**, 274009.
15 E. Cleiren, S. Heijkers, M. Ramakers and A. Bogaerts, *ChemSusChem*, 2017, **10**, 4025–4036.
16 M. Ramakers, G. Trenchev, S. Heijkers, W. Wang and A. Bogaerts, *ChemSusChem*, 2017, **10**, 2642–2652.
17 S. Pancheshnyi, B. Eismann, G.J.M. Hagelaar, L.C. Pitchford, Computer code ZDPlasKin, http://www.zdplaskin.laplace.univ-tlse.fr (University of Toulouse, LAPLACE, CNRS-UPS-INP, Toulouse, France), 2008.
18 I. T. Trotuş, T. Zimmermann and F. Schüth, *Chem. Rev.*, 2014, **114**, 1761–1782.
19 P. L. Spath and D. C. Dayton, *Preliminary Screening -- Technical and Economic Assessment of Synthesis Gas to Fuels and Chemicals with Emphasis on the Potential for Biomass-Derived Syngas*, Golden, CO (United States), 2003.
20 G. Trenchev, S. Kolev, W. Wang, M. Ramakers and A. Bogaerts, *J. Phys. Chem. C*, 2017, **121**, 24470–24479.
21 Q. Wang, B.-H. Yan, Y. Jin and Y. Cheng, *Plasma Chem. Plasma Process.*, 2009, **29**, 217–228.
22 J. Q. Zhang, J. S. Zhang, Y. J. Yang and Q. Liu, *Energy and Fuels*, 2003, **17**, 54–59.
23 M. E. Gálvez, A. Albarazi and P. Da Costa, *Appl. Catal. A*, 2015, **504**, 143-150.
24 T. Kozák and A. Bogaerts, *Plasma Sources Sci. Technol.*, 2014, **23**, 045004.
25 R. Snoeckx, A. Ozkan, F. Reniers and A. Bogaerts, *ChemSusChem*, 2017, **10**, 409–424.